AD-A078 628 AIR FORCE GEOPHYSICS LAB HANSCOM AFB MA F/G 4/1
SATELLITE ATMOSPHERIC RADIANCE MEASUREMENTS IN THE VACUUM ULTRA--ETC(U)
JUL 79 R E HUFFMAN , F J LEBLANC

UNCLASSIFIED AFGL-TR-79-0151 NL

| OF |
AD
A078628

END
DATE
FILMED
| — 80
DDC

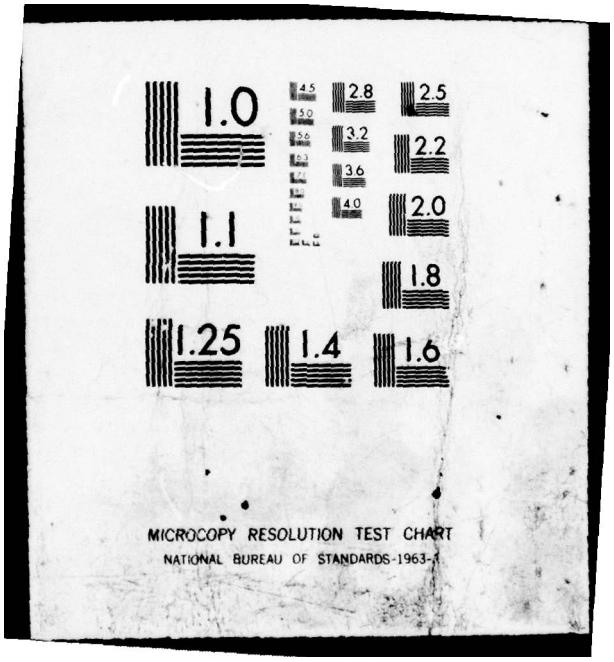
1.0
1.1
1.25
1.4
1.6
1.8
2.0
2.2
2.5
2.8
3.2
3.6
4.0
4.5
5.0
5.6
MICROCOPY RESOLUTION TEST CHART
NATIONAL BUREAU OF STANDARDS-1963-A

AFGL-TR-79-0151
ENVIRONMENTAL RESEARCH PAPERS, NO. 695

LEVEL II

Satellite Atmospheric Radiance Measurements in the Vacuum Ultraviolet

R. E. HUFFMAN
F. J. LoBLANC
J. C. LARRABEE
D. E. PAULSEN

5 July 1979

AERONOMY DIVISION PROJECT 6690

AIR FORCE GEOPHYSICS LABORATORY
HANSCOM AFB, MASSACHUSETTS 01731

AIR FORCE SYSTEMS COMMAND, USAF

This report has been reviewed by the ESD Information Office (OI) and is releasable to the National Technical Information Service (NTIS).

This technical report has been reviewed and is approved for publication.

FOR THE COMMANDER

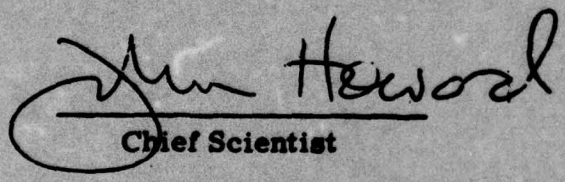

Chief Scientist

Qualified requestors may obtain additional copies from the Defense Documentation Center. All others should apply to the National Technical Information Service.

(12) 44

Unclassified

SECURITY CLASSIFICATION OF THIS PAGE (When Data Entered)

REPORT DOCUMENTATION PAGE	READ INSTRUCTIONS BEFORE COMPLETING FORM
(14) 1. REPORT NUMBER: AFGL-TR-79-0151, AFGL-ERP-665 / 2. GOVT ACCESSION NO.	3. RECIPIENT'S CATALOG NUMBER
(6) 4. TITLE (and Subtitle): SATELLITE ATMOSPHERIC RADIANCE MEASUREMENTS IN THE VACUUM ULTRAVIOLET	5. TYPE OF REPORT & PERIOD COVERED: Scientific. Interim.
	6. PERFORMING ORG. REPORT NUMBER: ERP No. 665
(10) 7. AUTHOR(s): R. E. Huffman, D. E. Paulsen, F. J. LeBlanc, J. C. Larrabee	8. CONTRACT OR GRANT NUMBER(s)
9. PERFORMING ORGANIZATION NAME AND ADDRESS: Air Force Geophysics Laboratory (LKO), Hanscom AFB, Massachusetts 01731	10. PROGRAM ELEMENT, PROJECT, TASK AREA & WORK UNIT NUMBERS: (16) 62101F, 66901701 (17) 17
11. CONTROLLING OFFICE NAME AND ADDRESS: Air Force Geophysics Laboratory (LKO), Hanscom AFB, Massachusetts 01731	(11) 12. REPORT DATE: 5 Jul 1979; 13. NUMBER OF PAGES: 43
14. MONITORING AGENCY NAME & ADDRESS(if different from Controlling Office): 409 578	15. SECURITY CLASS. (of this report): Unclassified; 15a. DECLASSIFICATION/DOWNGRADING SCHEDULE

16. DISTRIBUTION STATEMENT (of this Report)

Approved for public release; distribution unlimited.

17. DISTRIBUTION STATEMENT (of the abstract entered in Block 20, if different from Report)

(9) Environmental Research Papers,

18. SUPPLEMENTARY NOTES

19. KEY WORDS (Continue on reverse side if necessary and identify by block number)

Ultraviolet
Vacuum ultraviolet
Atmospheric radiation
Radiance
Airglow
Aurora
Scattering

20. ABSTRACT (Continue on reverse side if necessary and identify by block number)

A satellite experiment has obtained nadir-viewing atmospheric radiance measurements in the 1100 to 2900 angstrom wavelength region from the polar orbiting satellite S3-4. This report describes the instrumentation, measurement techniques, and initial results. The observed emission is from airglow, solar scatter, and auroral regions. Spectral and spatial measurements previously unavailable have been made for the nitrogen Lyman-Birge-Hopfield emission, vacuum ultraviolet aurora, hydrogen geocorona, tropical ultraviolet airglow, twilight fluorescence nitric oxide spectrum, and night oxygen CONT →

DD FORM 1 JAN 73 1473 EDITION OF 1 NOV 65 IS OBSOLETE

Unclassified

SECURITY CLASSIFICATION OF THIS PAGE (When Data Entered)

409 578 xlt

20. (Cont)

Herzberg band emission. Low values of the day and night background radiance values have been found; these values can be applied to improved missile detection techniques. Spatial resolution down to about one kilometer will enable possible variability to be sought. Observations were made in the period March to September 1978. Correlations with other geophysical factors such as solar flux, magnetic index, and seasonal variations will be made after the data base from the experiment is completed.

Preface

Individuals and organizations contributing significantly to the success of this experiment and to whom grateful acknowledgment is made are the following: Mr. R. Crabbs, Research Support Instruments, and Mr. E. F. Mackey, Spacom Electronics, Inc., who provided the instruments under Contract F19628-73-C-0028; Acton Research Corporation for the VUV interference filters; the Space Test Program Office of the Space and Missile Systems Organization, with special appreciation to Capt. K. Wright and Lt. H. Donald; Mr. R. Knauss, Aerospace Corporation; Mr. V. C. Baisley, AFGL(LKO); Mr. C. Reynolds and Capt. D. Davenport, AFGL(LC); Mr. R. McInerney, AFGL(SUWA); and Mr. J. Higgins, AFGL West Coast Office; Mr. Denis Delorey, Boston College; Mr. J. Davis, Spacom Electronics; Lockheed Missiles and Space Company, and the Space and Missile Test Center.

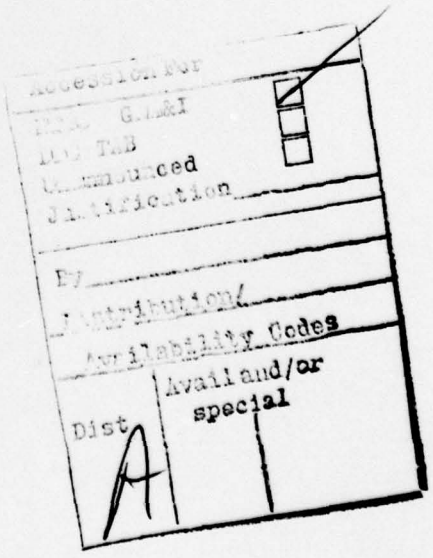

Contents

Illustrations

Tables

Satellite Atmospheric Radiance Measurements in the Vacuum Ultraviolet

1. INTRODUCTION

1.1 Overview

The Vacuum Ultraviolet Backgrounds experiment was flown successfully on the SAMSO Space Test Program satellite S3-4 during the period March to September 1978 in a polar, sun-synchronous orbit. All major objectives were achieved with over 700 hours of data obtained for the planned spectral range (1100 to 2900 Å) and spatial resolution (to approximately 1 kilometer). This large body of new atmospheric information will require several years to be analyzed completely. At present, the records are fairly complete for March and April 1978. This report describes the experiment and these initial results.

1.2 Rationale

Utilization of the ultraviolet regime of the spectrum (wavelengths shorter than about 4000 Å) for military applications requires improved knowledge of the fundamental geophysical properties of the atmosphere. Applications include missile detection and surveillance, technical intelligence, ionospheric monitoring, horizon determination, and many other remote sensing tasks. For these purposes, the spectral, spatial, and temporal characteristics of the disturbed and undisturbed

(Received for publication 3 July 1979)

atmosphere must be known, as they form the background, or radiative environment, necessarily associated with any application.

It is important to emphasize that the goal of this work is not simply to gather more observations of the airglow. The primary goal is to measure the neglected regions of low radiance that will prove most valuable for applications. Use of the ultraviolet requires that these low radiance levels be known both day and night. Moreover, those regions dominated by solar scattering have also been neglected in previous investigations. The present experiment has been designed to measure these less well-known regions, in order to begin acquisition of the detailed scientific understanding necessary for optimal utilization.

1.3 Impact on Current Problems

This work is closely related to the development of missile surveillance and tracking systems through measurement of missile exhaust plumes in the ultraviolet also being conducted at the Air Force Geophysics Laboratory. The first measurements on large engines were successfully completed under Project Chaser.[1] Since that time, work has been under way for detailed observations[2] of bus and vernier engines on the Multispectral Measurements Program.

A workable missile observation technique must consider both the target intensity and background properties, in order to achieve a proper signal-to-background ratio. The two elements of this problem are being obtained by a combination of our rocket and satellite results. These results lead to a significant lowering of the known background levels in the region of the oxygen minimum near 1500 Å to a maximum of about 1.3 kR at midday and to less than 1 R at the night minimum. In addition, the importance of the opaqueness of the lower atmosphere to the vacuum ultraviolet (VUV) is recognized as an advantage because VUV systems cannot be blinded or given false alarms from the ground.

Remote sensing of atmospheric number density is being investigated in several ways: Oxygen atom densities will be obtained from the Herzberg bands in our data. The present use of the (1, 0) nitric oxide band fluorescence to obtain its number density has been questioned in the auroral zone from improved rocket spectra. The present satellite data confirm this difference by separating the twilight from the auroral spectra. Thus, better definition of the use of the technique will be possible. In

---

1. Draper, J.S., Bien, F., Huffman, R.E., and Paulsen, D.E. (1975) Rocket plumes in the thermosphere, AIAA Journal 13:825-827.

2. Russak, S.L., Flemming, J.C., Huffman, R.E., Paulsen, D.E., and Larrabee, J.C. (1979) Development of Proximity and Electrostatically Focused Digicons for UV Measurements from Sounding Rockets, AFGL-TR-79-0006, AD A068086.

this manner, remote sensing applications such as planned on the NASA Upper Atmosphere Research Satellites program will be improved. In addition, correlation with the atmospheric mass density measured by the Rotatable Calibration Accelerometer (ROCA)[3] and by the Cold Cathode Gauge/Particle Flux Accumulator of the same flight will also be investigated.

There is a growing awareness of the role that ultraviolet sensors can play in ionospheric monitoring for improvement of radio wave communications and surveillance. Applications for these data extend both to the auroral regions and to equatorial disturbed ionospheres; for example, VUV sensors can detect and measure aurora both day and night, and the sensitivity of the instruments enables previously unsuspected regions of particle precipitation to be observed. The new observations are being used to design experiments for the Auroral E rocket program and for study of the continuous aurora relative to operation of over-the-horizon radar.[4] The auroral locations match Defense Meteorological Satellite Program (DMSP) auroral photographs, and demonstrate the feasibility of the auroral detector proposed for the DMSP several years ago.

The observations are also applicable to atmospheric nuclear effects research; for example, observations were made near Kwajelein Island during the DNA Wideband Support program in July and August 1978. In the vacuum ultraviolet, the night tropical airglow is observed and correlations with the Pulsed Plasma Probe experiment also on S3-4 will be made.[5] Although our experiment was not optimized for this use, an initial survey demonstrates strong but variable tropical airglow from the oxygen ion-recombination lines at 1304 and 1356 Å.

1.4 Future Efforts

While many facets of the global radiance of the earth are being defined by the VUV Backgrounds experiment, other observations were precluded because of limitations such as viewing direction, altitude, and local time availability. Chief among these is the altitude variation of the atmospheric radiance- or horizon-limb profile as seen from space. From the nadir-viewing data, reconstruction of this profile at a specific wavelength is impossible. It is necessary to develop improved horizon sensing techniques for spacecraft and also for many of the most useful

3. Marcos, F. A., and Champion, K. S. W. (1979) Satellite Density Measurements with the Rotatable Calibration Accelerometer (ROCA) AFGL-TR-79-0005, AD A069740.

4. Whalen, J. A., and Sharber, J. R. (1979) Integration over the loss cone of electrons in the continuous (diffuse) aurora: Gaussian latitudinal profile, Trans. Am. Geophys. Union 60:355.

5. Szuszczewicz, E. P., Holmes, J. C., and Walker, D. N. (1979) On the probing of ion and electron irregularity spectra, Trans. Am. Geophys. Union 60:339.

remote sensing applications. Plans therefore have been made to obtain the horizon limb profiles in the ultraviolet during a number of shuttle sortie flights as a part of the experiment AFGL-801, Horizon Ultraviolet Program.

2. EXPERIMENT

2.1 Orbital Characteristics

The Vacuum Ultraviolet Backgrounds satellite experiment consists of a spectrometer, a photometer, and an electronics module (Figure 1). Drawings are shown in Figures 2 and 3, and specifications are provided in Table 1. The instruments will be presented in the order named.

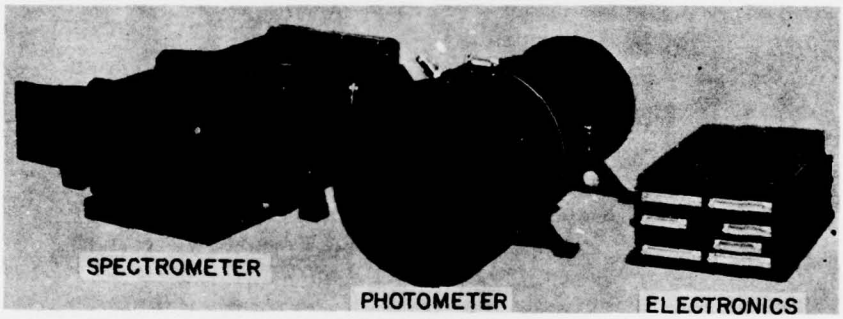

Figure 1. Flight Instruments for the Vacuum Ultraviolet Backgrounds Experiment

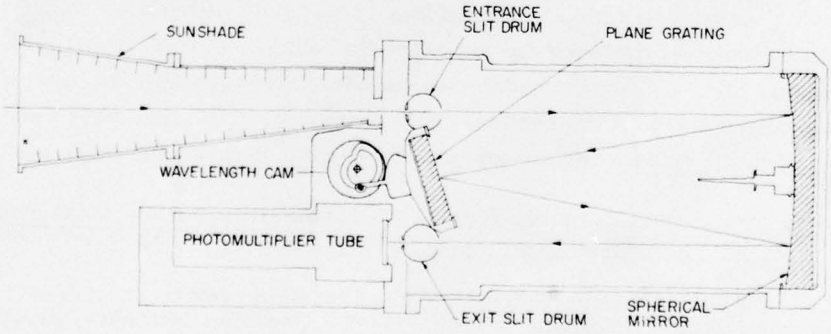

Figure 2. Schematic Drawing of VUV Backgrounds Spectrometer

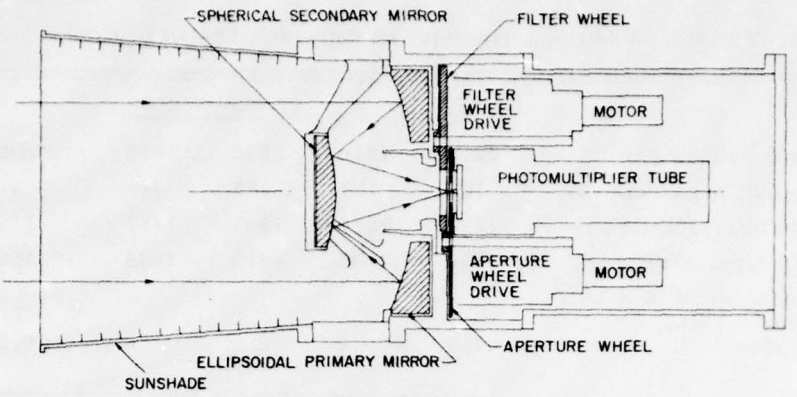

Figure 3. Schematic Drawing of VUV Backgrounds Photometer

Table 1. Vacuum Ultraviolet Backgrounds Sensors

	Spectrometer	
Type	Dual Ebert-Fastie 0.25 meter, f/5	
Scan	Simultaneous from short to long wavelength, rapid flyback	
Scan time	Approx. 22-sec total, including 2.8-sec flyback	
Bandpass, FWHM	25, 5, 1 Å or pinhole for each range	
View direction	Toward earth center to within about 1°	
Field-of-view	11.5° square	
Observed area/Transit time	Approx. 20-km square at 100-km altitude (satellite at 200 km) 20 km in 2.7 sec	
Ground track/scan	163 km (1.5° latitude at equator)	
Range designation	VUV	UV
Wavelength limits (Å)	1070-1930	1620-2900
Detector/counting period	EMR 542G-08/5 msec	EMR 542F-08/5 msec
Photocathode/window	CsI/LiF	CsTe/LiF
Noise equivalent (R/Å) (preflight, < 1 c/s) (25Å)	$<7 \times 10^{-4}$ (1216 Å)	$<1 \times 10^{-3}$ (2500 Å)
	Photometer	
Detector/counting period	EMR 542G-09/10 msec	
Photocathode/window	CsI/MgF_2	
Direction of view	Toward earth center to within about 1°	
Optics	f/1, ellipsoidal primary, convex spherical secondary	

Table 1. Vacuum Ultraviolet Backgrounds Sensors (Cont)

	Photometer				
Interference Filters (Å)	1216	1340	1550	1750	no filter
Full width half maximum (Å)	116	151	165	146	401
Wavelength Min, FWHM (Å)	1194	1274	1485	1677	1197
Wavelength Max, FWHM (Å)	1310	1425	1650	1823	1598
Noise Equivalent ($R/Å \times 10^{-5}$) (preflight, < 1 c/s, max aperture)	<1.2	<0.54	<2.9	<4.8	<0.04
Aperture full angle	5.9°		1.65°	0.46°	0.12°
Spatial field at 100 km alt.	10.5 km		2.9	0.80	0.20 (Sat. at 200 km)
Max Observation time	1.4 sec		0.39	0.11	0.027
Max counting periods (FMT.A)	140		39	11	2.7

First, the spectrometer consists of two 1/4 m, f/5, Ebert-Fastie units scanned in wavelength by a shared grating drive. The shorter wavelength VUV range was from about 1070 to 1930 Å, and the longer wavelength UV range from about 1620 to 2900 Å. The dual ranges are observed simultaneously from short to long wavelength with a total cycle time of about 22 sec, including a rapid flyback to the starting point after each scan. For each range, 1, 5, and 25 Å bandwidth slits are available. The slit drums had a pinhole position in order to obtain dark count readings.

In front of the entrance slit a sunshade was used (Figures 1 and 2), but no telescope or collector was incorporated in the spectrometer. The detectors were EMR photomultipliers. For the VUV range, the 542G-08 tube with a cesium iodide photocathode was used and for the UV range, the 542F-08 tube with a cesium telluride photocathode; both tubes had lithium fluoride windows. All observations were made using photon-counting detection. Figure 4 gives the laboratory sensitivity in counts per photon for each range as measured at AFGL before integration into the spacecraft. The curves are largely determined by the photocathode material, except at less than 1200 Å, where the MgF_2 coated optics efficiency is a factor owing to decreased reflectivity.

The counting period for data collection is 5 msec, based on timing from the spacecraft clock. The counts observed during this period are accumulated in a 12-bit counter and then at the conclusion of each counting period they are shifted in less than 1 μsec to a register for readout before the end of the next period. At the time the counter readings are shifted, separate pulses move the stepper motor, rotating the two gratings to the next position and moving a wavelength counter ahead

one unit. For each 5-msec period, the VUV counts, UV counts, wavelength counter reading, and slit position code are sent into the data stream. Temperatures and voltages complete the data telemetered for the spectrometer. The photomultipliers are operated with a fixed high voltage in the pulse saturation region.

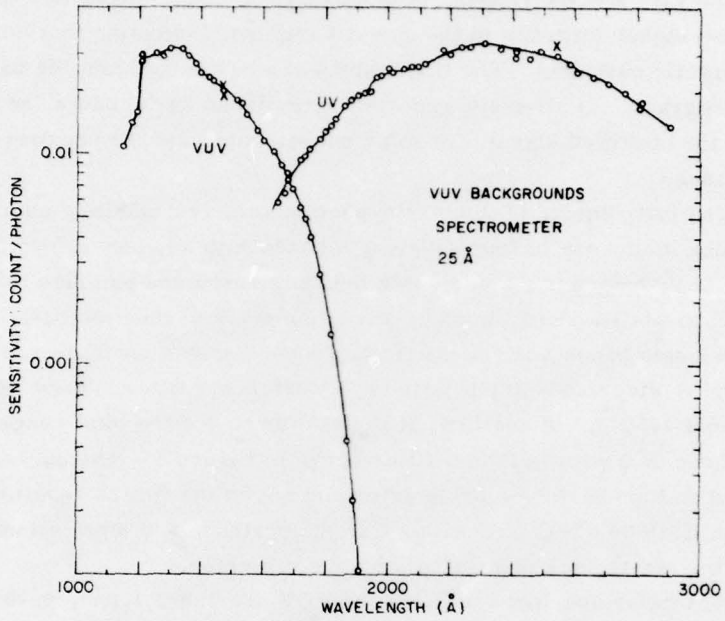

Figure 4. Spectrometer Sensitivity vs Wavelength

When the experiment is "on", the spectrometer continuously performs its wavelength and flyback cycle; in other words, each wavelength of a range is sampled once every 22 sec or about every 1.5 degrees of latitude at the equator for the ground speed of about 7.4 km/sec. The flyback requires about 2.8 sec and the forward scan 19.2 sec.

The minimum noise equivalent spectral radiance (NESR) of the spectrometer with the largest entrance slit of 25 Å full width half maximum (FWHM) can be approximated using a dark count of one count per second. The preflight dark count for laboratory conditions was always less than this, being about 0.6 and 0.8 count/sec for the VUV and UV ranges, respectively. The flight values are larger, as given in the next paragraph. For the VUV range at the 1216 Å Lyman alpha line of the hydrogen atom, the NESR is 56 photon/(sec cm^2 ster Å). For the UV range near 2500 Å, the NESR is 82 photon/(sec cm^2 ster Å). The NESR is also a function of

wavelength, although it is less variable for the UV range (Figure 4). For the VUV range, the decreasing quantum efficiency of CsI toward longer wavelengths leads to an increase in the NESR. The noise equivalent in Rayleigh per angstrom is given in Table 1.

The dark count observed in flight outside auroral regions is about 6 and 7 counts per sec for the VUV and UV ranges, respectively. Count rates up to 7 times higher are seen at the higher latitudes in the auroral regions, indicating that the increase is due to energetic particles. The flight NESR can be scaled from the values in the preceding paragraph. In all cases reported here, these dark counts are insignificant compared to the observed signal. In some cases, correction for scattered light may be necessary.

The second instrument, (Table 1) the photometer, is capable of obtaining atmospheric radiance in any one of five wavelength bands with any one of four fields-of-view (FOV). It therefore has a very wide dynamic range and can give information about spatial variability along the nadir-direction track of the satellite.

The wavelength bands and sensitivity of the photometer are shown in Figure 5. The 116 to 164 Å wide bands are isolated by interference filters peaked at 1216, 1340, 1550, and 1750 Å. In addition, it is possible to use the total range of the CsI photocathode as shown in the no-filter curve in Figure 5. The curves illustrated were obtained on the assembled photometer and not on the filters separately. The detector is an EMR 542G-09 tube with a CsI photocathode and MgF_2 window with photon-counting electronics identical to the spectrometer.

The four circular apertures defining the FOV are 5.9°, 1.65°, 0.46°, and 0.12° (diameter), and are centered on the optics axis. The smallest fields-of-view were set to allow search for spatial structure in the VUV background down to approximately one kilometer. The largest aperture position was set to allow detection of weak earth backgrounds during the night. There is a factor of about 12 in sensitivity between adjacent aperture positions, which allows them also to be used to adjust the sensitivity over a range of 2×10^3.

The photon counts observed are accumulated and transmitted in a manner similar to that for the spectrometer, with exception of the counting period—10 msec (Format A) or 7.5 msec (Format C). In addition to the photon count data, the telemetry records also included the filter and aperture identifications plus temperatures and voltages. A fixed high voltage in the pulse saturation regime was used for the photomultiplier.

The two-element f/1 telescope (Figure 3) consists of an ellipsoidal primary collecting mirror and a convex spherical secondary mirror (Dall-Kirkham system) which focuses the field onto the aperture through a nonlimiting hole in the center of the collector mirror. The filters and field-limiting apertures are contained in separate disks or wheels placed immediately behind the collector and in front of

the photomultiplier cathode. The aperture wheel also contains a blank position that allows dark counts to be observed.

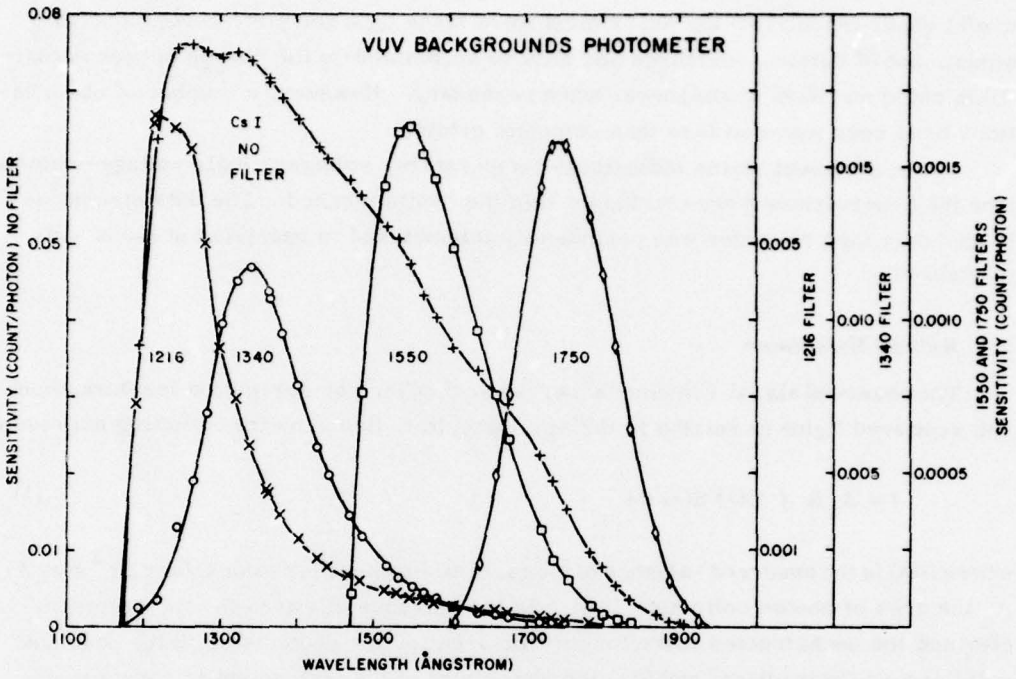

Figure 5. Photometer Filter Sensitivity vs Wavelength

The photometer NESR can be approximated for the 5.9° diameter FOV with a noise count of 1 count per second. The preflight value was 0.5 count per second. In units of photon/(sec cm^2 ster Å), these are 1216 Å:0.92; 1340 Å:0.43; 1550 Å:2.3; 1750 Å:3.8; and no filter:0.03. The flight value of the dark count is 4 counts per sec (nonauroral) and 25 counts per sec (auroral). All these rates are generally too low to be significant for measurements reported herein. The noise equivalent in R/Å is given in Table 1.

2.2 Orbital Characteristics

The VUV experiment was flown on the DOD satellite S3-4 in a polar, near-circular orbit with a three-axis stabilized platform. The center of the instrument FOV was pointed toward the center of the earth to within less than 1° during all data acquisition periods. The inclination was about 96.5°, making it near sun-synchronous. The local times of the ascending and descending nodes at the equator were approximately constant at about 2230 and 1030, respectively.

The altitude varied from about 260 to 160 km. Routine observations were obtained for almost every day between 30 March and 10 September 1978. The most useful observations for the experiment were made on a complete revolution, with adjustment of filters, apertures and slits to accommodate the change between solar-illuminated and dark atmosphere, when necessary. However, a number of observations have been made on less than complete orbits.

The experiment status indicators—temperature, voltages, logic voltage—showed that the observations were obtained within the limits planned. The data stream as stored on a tape recorder was periodically telemetered to receiving stations and processed.

2.3 Radiance Measurement

The observed signal I in counts per second (after any correction for dark count and scattered light) is related to the atmospheric radiance by the following expression:

$$I = A_c \Omega \int B(\lambda)\, S(\lambda)\, d\lambda \qquad (1)$$

where $B(\lambda)$ is the observed radiance of the earth atmosphere in photons/(sec cm^2 ster Å); A_c the area of photon collection, which is the entrance slit area for the spectrometer and the unobstructed collector mirror area for the photometer; Ω the observed solid angle in steradians; and $S(\lambda)$ the sensitivity of the instrument in counts per photon.

The sensitivity $S(\lambda)$ includes not only the quantum efficiency of the photomultiplier but also reflection and grating efficiencies (see Figures 4 and 5). For the spectrometer, S does not vary appreciably across the bandpass and therefore it can be removed from the integral. For the photometer, $S(\lambda)$ is integrated over the wavelength range of appreciable response.

The radiance $B(\lambda)$ may exhibit considerable variation with wavelength in the vacuum ultraviolet and ultraviolet. In many cases this variation is not known in detail initially and it must depend on spectrometer data to provide the wavelength resolution required to determine $B(\lambda)$ more fully. As the first step in data analysis, we neglect this variation and consider $B(\lambda)$ to be constant across the spectral interval for both spectrometer and photometer data. Therefore, $B(\lambda)$ is removed from the integral. For some wavelength regions, further allocation among the spectral features within the bandpass may be made.

Results also may be given in terms of the column emission rate in Rayleighs, which is equal to $B(\lambda)\ 4\pi\ \Delta\lambda / 10^6$, where $\Delta\lambda$ is the bandwidth or filter FWHM in angstroms.

2.4 Calibration and Accuracy

The ultraviolet calibration of the instruments was achieved using the UV calibration facility developed at AFGL in connection with the rocket Multispectral Measurements Program. The facility is described in more detail in relation to the development of digicon spatial detectors for spacecraft use under that program.[2]

An instrument was placed in the collimated beam vacuum chamber where it was illuminated by collimated light of known intensity (photon/sec cm^2). From the counts observed by the instrument and its known collection aperture A_c, the sensitivity in counts per photon was obtained. The instrument was then moved independently in azimuth and elevation over a range of ± 30 degrees so that the response throughout, as well as outside the field-of-view, could be obtained. In this way, Ω or the solid angle observed by the instrument was found as the half-width of the response curve normalized to the optic axis reading; unacceptable levels of out-of-field response could also be found.

Two types of light source are used. One type is an approximation to a point source consisting of a small gas discharge tube primarily emitting one of the following lines: 1216 Å, H Lyman alpha; 1470 Å, Xe resonance line; or 2537 Å, Hg resonance line. These sources have sufficient intensity to search for out-of-field response but only at a single wavelength. On the other hand, wavelength variation but with less intensity has been obtained with a gas discharge using He gas with a trace of CO_2 added. The strong emission bands of the CO fourth positive system and of other discharge emitters produced sufficient coverage. The lamp was used with a small vacuum monochromator having a circular exit aperture. Either the point discharge source or the monochromator exit aperture was placed at the focus of the collimating mirror with the aid of a folding mirror. A 38-cm diam beam is produced with the point sources.

The beam is mapped with a beam probe photomultiplier that can be moved in horizontal and vertical directions throughout the area of the beam. An EMR 542F-08 tube which has a CsTe photocathode and LiF window is used. The counting electronics and power supply are very similar to the flight units. After measurement of beam intensity, the probe is stored outside the beam while the flight instrument is tested.

The radiometric calibration is based on a secondary standard photodiode obtained from the National Bureau of Standards (NBS). The beam probe photomultiplier is calibrated against the diode in a separate vacuum chamber on a Seya-Namioka monochromator. A series of neutral-density filters of known transmittance is utilized. The NBS photodiode is returned periodically for recalibration, and the changes between adjacent recalibrations are never more than a few percent. The beam probe is periodically calibrated against the NBS photodiode.

The sensitivity $S(\lambda)$ is found to be constant over a large dynamic range of up to about 10^6 counts per second. This measurement is made on the collimated beam system using a set of neutral density filters of known transmission between the light source and the folding mirror. The response curve was also measured in the nonlinear region so that the occasional observations in this region are correctable. Nonlinearity is found at high count rates due to the saturation of the counting electronics.

The accuracy of radiance determination can be discussed using Eq. (1). The largest uncertainty is in determination of the sensitivity $S(\lambda)$, which is based on the accuracy of the NBS photodiode calibration and our transfer of it to the flight instruments. The photodiode accuracy is given by NBS as follows:

1164-2000 Å, 6% probable error,
2067-2296 Å, 8% probable error,
2385-3200 Å, 10% probable error.

We transfer this calibration first to the beam probe using neutral density filters of known transmission to reduce the light intensity from levels suitable for the photodiode. Then the transfer is made from the beam probe to the flight instrument. The transfer uncertainty, defined as the square root of the sum of the squares of individual uncertainties is 6.7 percent for all wavelengths except (1) 1800 to 2300 Å, where the value is 11.7 percent due to weaker emission lines in the source, and (2) 1216 to 1153 Å, where an additional step increases the value to 12.0 percent. The error from the transfer and the NBS probable error must then be combined to give the total estimated uncertainty in $S(\lambda)$.

The remaining items in Eq. (1) contribute much less to the error budget. The collection aperture A_c is known to better than 2 percent; the solid angle Ω is known to about 3 percent; and the wavelength or wavelength range is known to less than 1 percent. The number of counts observed has the normal counting uncertainty as well as possible added uncertainty due to the subtraction of dark counts and scattered light, if these are significant. For the most favorable measurement conditions, under discussions here, the latter two items are neglected. The number of counts is assumed to be at least 1000, and thus within the linear dynamic range, so that the counting uncertainty is less than 3 percent.

These errors when combined as before led to the following over-all estimated uncertainties.

Wavelength (Å)	Value (%)
1153 - 1216	13.9
1216 - 1800	9.7
1800 - 2000	13.7
2000 - 2296	14.7
2385 - 2900	12.6

Therefore, under most favorable conditions, the radiance uncertainty is less than 15 percent over the entire range. Wavelengths less than 1153 Å will be discussed in future reports.

Less favorable situations will increase the uncertainty; for example, scattered light will lead to an increase in the uncertainty for the smallest radiance values found between strong emission features in daytime. In the search for weak emission sources, the dark count over the polar regions might become significant. Again, the uncertainty due to low counts may become important in some cases. Finally, day measurements at the smallest solar zenith angle (SZA) may be above the linear dynamic range of the pulse-counting electronics. For these less than optimum conditions, a larger uncertainty will be stated.

The possibility of polarization effects in the calibration or on-orbit observations is not believed to be serious as a result of a few simple observations during calibration. However, final definition of this effect is still open and additional tests on similar gratings may lead to an additional uncertainty estimate from this source in the future.

A major factor which may affect the observation is contamination of the optics after calibration, both in the integration phase and in orbit. To monitor changes in sensitivity, test lamps were built into the spectrometer and photometer to measure relative response in tests before spacecraft integration. Due to spacecraft limitations, it was not possible to use these after installation of the instrument in flight position, and for this phase a fixture containing three discharge tubes similar to the laboratory point sources was used. The unit had 1470 Å lamps for the spectrometer VUV range and the photometer and a 2537 Å lamp for the spectrometer UV range. The flight instruments were purged with a flow of high-purity nitrogen to remove oxygen and water vapor during these tests. No significant change in instrument response within the fairly large random scatter was found during spacecraft integration and test, which included checks to about two months before launch.

To date, there is no evidence of change in sensitivity during the on-orbit observation period as detected by a drift in the average undisturbed radiance values. However, few records from the end of the flight are available. The records also do not indicate any observation of solar radiation scattered by spacecraft structure. This demonstrates the effectiveness of the sunshades.

3. RESULTS

3.1 Basic Description

When the Vacuum Ultraviolet Backgrounds experiment is operating, the spectrometer acquires VUV and UV records simultaneously, and the photometer observes with the selected filter and aperture. The spectrometer (slits) and the photometer (filter and aperture) were designed for the sampling of a wide range of radiance values. In order to prevent excessive photomultiplier currents, smaller apertures and slits were used generally during the day. The records analyzed here are based primarily on observations of complete orbits obtained in March and April 1978. Other types of records cover only portions of an orbit. The data from the five and one-half month flight will be analyzed as available in order to establish longer term variations and possible correlation with K_p, solar flux, season, and so on.

In this report, we describe our observations of the total global radiance profiles for the four VUV filter bands in the photometer. We also describe intensities of the Lyman-Birge-Hopfield bands of molecular nitrogen, spatial structure in the VUV auroral region, intensities in the hydrogen Lyman-alpha geocorona, and new details concerning the oxygen tropical airglow. To date, several other initial observations have been included. The following will be examined in more detail in later reports upon analysis of sufficient reduced data: variation of the molecular oxygen Herzberg bands at night; comparison of high-latitude twilight and auroral spectra to aid in distinguishing the "2150 A" feature in both regions; and comparison of auroral and mid-latitude day spectra.

The most similar previous satellite observations appear to be the UV spectrometer[6] and UV ion cells[7] on the Ogo-4 satellite. The results from our experiment demonstrate improved wavelength resolution, higher sensitivity, and improved spatial resolution. Other rocket and satellite observations will also be discussed when appropriate.

3.2 Photometer Global Radiance Levels

The wavelength bands available on the photometer are described for convenience by nominal wavelengths 1216, 1340, 1550, and 1750 Å. However, these filters have an appreciable half-width of from 116 to 165 Å and they therefore detect several emitters. Table 2 describes the principal sources contributing to the observed

---

6. Barth, C.A., and Mackey, E.F. (1969) Ogo-4 ultraviolet airglow spectrometer, IEEE Trans on Geoscience Electronics GE7(2):114-119.

7. Chubb, T.A., and Hicks, G.T. (1970) Observations of the aurora in the far ultraviolet from OGO-4, J. Geophys. Res. 75:1290-1311.

radiance in each case. This observation of several emission features by each filter must be kept in mind when interpreting the data, especially for the 1216 and 1340 Å filters, where H Lyman alpha and the oxygen resonance multiplets (1304, 1356 Å) are not clearly separated. The 1550 Å and 1750 Å filters do completely eliminate the oxygen emission, since the filter is completely opaque at wavelengths less than about 1400 Å. Use of the spectrometer results allows a separate radiance level to be assigned each emission feature.

Table 2. Vacuum Ultraviolet Backgrounds Photometer: Wavelength Bands and Major Emitters

Filter Number	Designation	Full Width Half Maximum Å	Emitters (in order of importance)
1	1216	116	H 1216, O 1304, O 1356
2	1340	151	O 1304, O 1356, H 1216, N_2 LBH
3	1550	165	N_2 LBH, N 1493, Rayleigh scatter
4	1750	146	N_2 LBH, Rayleigh scatter

Figures 6, 7, 8, and 9 give the typical behavior of the earth's radiance in the four photometer bands. The counts per 10-msec period have been averaged over 5-sec intervals and then converted to radiance with the units of photons/(sec cm^2 ster Å). It is assumed for this conversion that there is no wavelength dependence of the radiance across the filter band. This, of course, is never exactly true, but it is a useful first procedure. Later the curves will be apportioned to specific emission sources using spectrometer data. The radiance values are plotted as a function of time over the complete orbit. Vertical dashed lines divide day and night conditions. These are the times when the spacecraft leaves or enters the earth's shadow.

Each photometer record shows abrupt peaks and other disturbances at locations in the general region of the auroral oval that are due to aurora. Some maxima are shown in corrected geomagnetic latitude. The detailed shapes and intensities vary greatly among orbits with the same filter, but auroral observations are seen to some degree on all orbits. The general shape of the curves exhibits weaker backgrounds at night, as expected. In addition, the figures demonstrate different relationships to the solar zenith angle among the filters. The tropical, or equatorial, ultraviolet airglow can be seen in several cases (Figures 6 and 7).

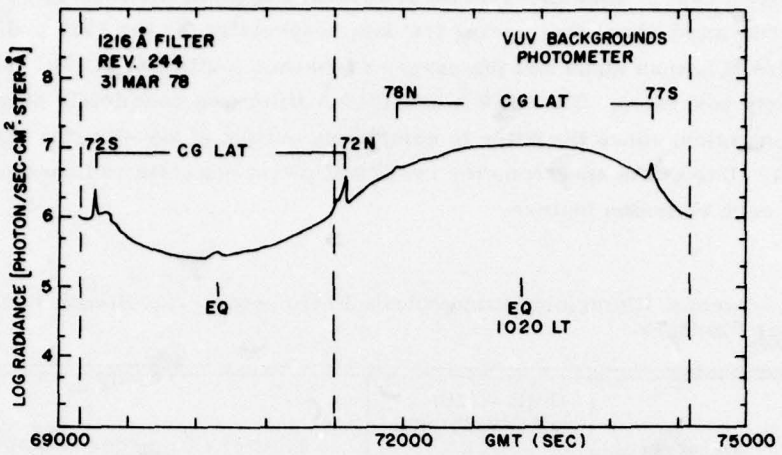

Figure 6. Photometer Global Survey (1216 Å Filter)

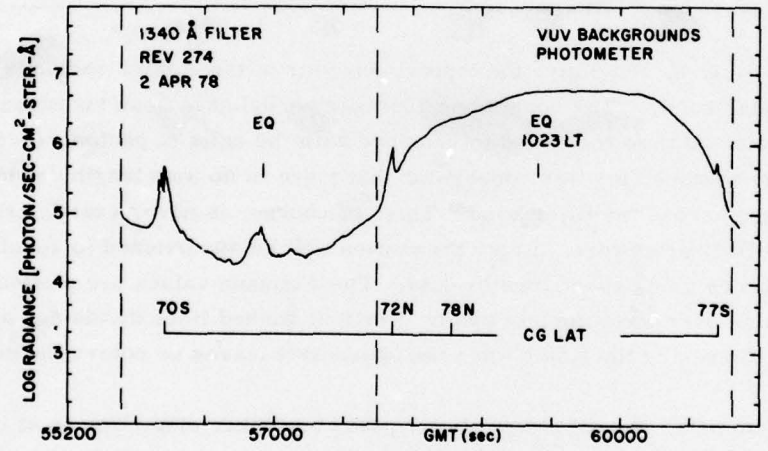

Figure 7. Photometer Global Survey (1340 Å Filter)

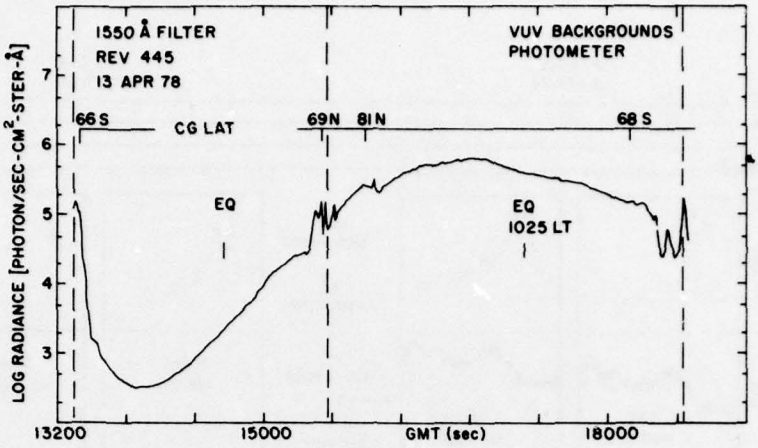

Figure 8. Photometer Global Survey (1550 Å Filter)

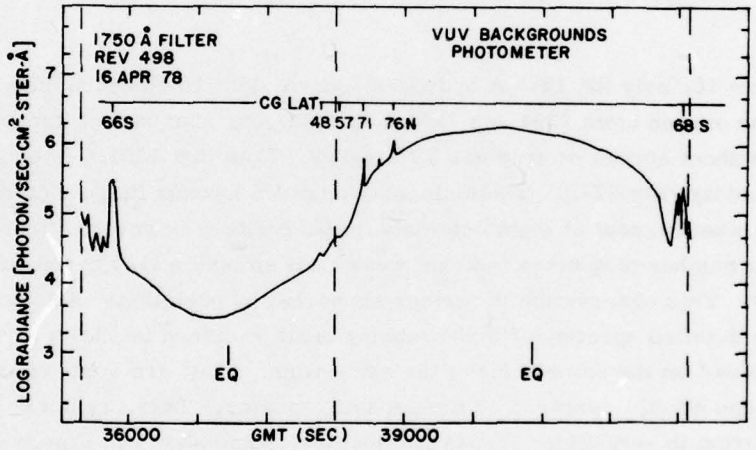

Figure 9. Photometer Global Survey (1750 Å Filter)

3.3 Atmospheric Spectra

The simultaneous observations of the VUV and UV ranges by the spectrometer are illustrated in Figure 10. These are photographs of microfiche records having every tenth point plotted. The upper frame is VUV and the lower is UV. The microfiche are useful in surveying the general observations rapidly and in this case to demonstrate qualitative differences found throughout the orbit. The intensity scale is logarithmic in counts per frame.

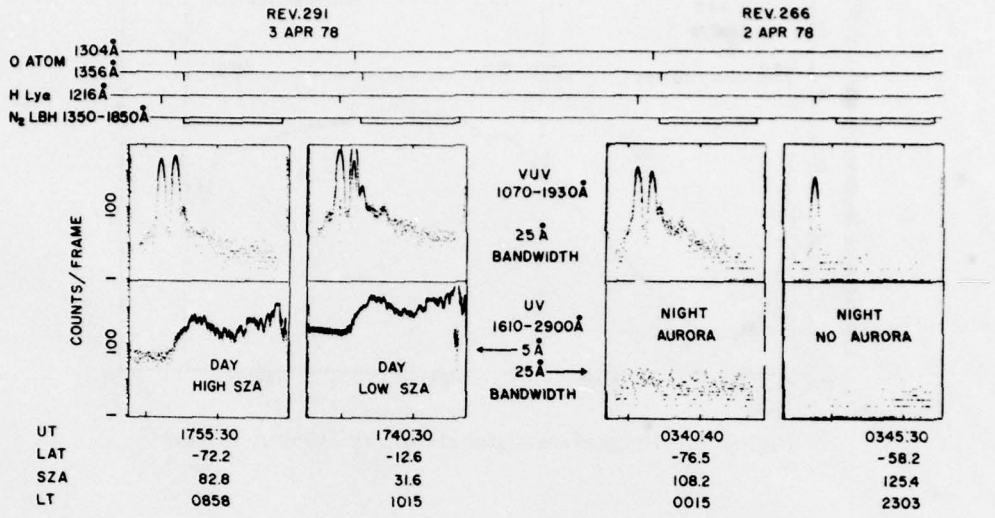

Figure 10. Spectrometer: Typical Microfiche Data

In Figure 10, only the 1216 Å hydrogen Lyman alpha line occurs under all conditions. The oxygen atom 1304 and 1356 Å lines appear everywhere except at night in regions without aurora or tropical UV airglow. Note that 1304 Å is brighter than 1216 Å at midday (low SZA). The molecular nitrogen Lyman-Birge-Hopfield (LBH) bands are present except at night outside auroral regions; however, Figure 8 and sums over a number of spectra indicate weak LBH emission also in the northern night sector. This observation is further supported by photometer data at 1750 Å.

A more detailed spectrum for the midday earth radiance is shown in Figures 11 and 12, obtained on the same orbit at the same time. They are sums of 10 and 5 spectra, respectively, centered on the geodetic equator. They are not corrected for the variation in sensitivity across the spectral range shown in Figure 4.

From spectra such as Figures 11 and 12 and other larger scale sums of spectra, it has been possible to identify the features given in Table 3. Methods to reduce further the scatter in the points such as sliding averages are being used; it is likely that more features will be classified in the future. The emission features observed in these midday observations are believed to be essentially identical with previous observations except that additional Lyman-Birge-Hopfield bands are observed. In addition, oxygen Schumann-Runge bands in absorption and Fraunhofer lines are observed.

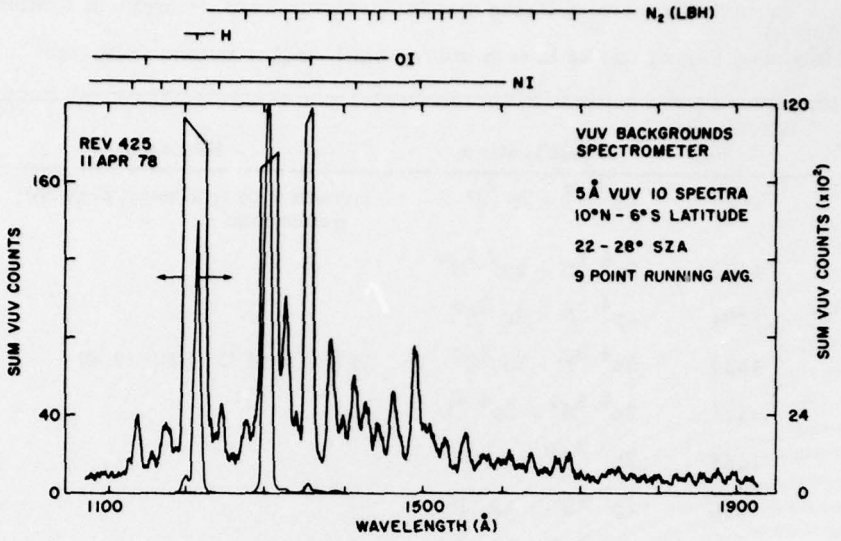

Figure 11. Spectrometer: 5 Å Data in VUV at Midday

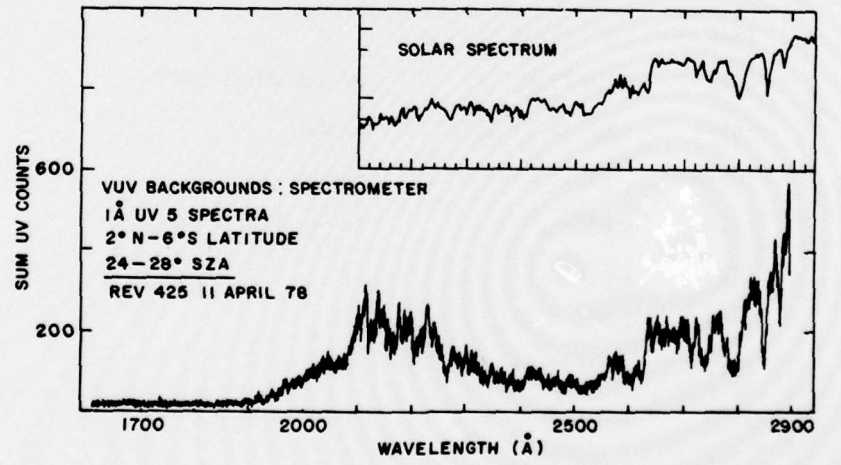

Figure 12. Spectrometer: 1 Å Data in UV at Midday

Table 3. Vacuum Ultraviolet Backgrounds Spectrometer: Prominent Features (1100-2900 Å)
(Observed during day at lowest solar zenith angle, unless indicated)

Emitter	Wavelength (Å)	Identification	Remarks
H	1216	$1s\ ^2S^o - 2p\ ^2P$	Lyman alpha; always present; geocorona
O	1152	$2p^4\ ^1D - 3s'\ ^1D^o$	
O	1304	$2p^4\ ^3P - 3s\ ^3S^o$	
O	1356	$2p^4\ ^3P - 3s\ ^5S^o$	Blend with N_2 LBH (3, 0)
N	1134	$2p^3\ ^4S^o - 2p^4\ ^4D$	
N	1168	$2p^3\ ^2D^o - 3d\ ^2F$	
N	1200	$2p^3\ ^4S^o - 3s\ ^4P$	
N	1243	$2p^3\ ^2D^o - 3s'\ ^2D$	
N	1412	$2p^3\ ^2P^o - 3s'\ ^2D$	Blend with N_2 LBH (4, 2)
N	1493	$2p^3\ ^2D^o - 3s\ ^2P$	Blend with N_2 LBH (3, 3)
N_2	1273	LBH (6, 0)	$a\ ^1\pi_g - X\ ^1\Sigma^+_g$
N_2	1325	LBH (4, 0)	
N_2	1339	LBH (5, 1)	
N_2	1354	LBH (3, 0)	Blend with O 1356
N_2	1382-4	LBH (5, 2) (2, 0)	Blend
N_2	1396-8	LBH (6, 3) (3, 1)	Blend
N_2	1412	LBH (4, 2)	Blend with N line
N_2	1430	LBH (2, 1)	
N_2	1444	LBH (3, 2)	
N_2	1464	LBH (1, 1)	
N_2	1493	LBH (3, 3)	Blend with N line
N_2	1508	LBH (4, 4)	
N_2	1515	LBH (1, 2)	
N_2	1530	LBH (2, 3)	
N_2	1554	LBH (0, 2)	

Table 3. Vacuum Ultraviolet Backgrounds Spectrometer: Prominent Features (1100-2900 Å) (Cont)

Emitter	Wavelength (Å)	Identification	Remarks
N_2	1626	LBH (1, 4)	
N_2	1688	LBH (1, 5) (5, 8)	
N_2	1690-2100	LBH	Numerous additional weak bands
N_2	2200-2800	Vegard-Kaplan bands	A $^3\Sigma_u^+$ - X $^1\Sigma_g^+$, aurora
NO	2000-2700	Gamma bands	A $^2\Sigma^+$ - X $^2\Pi$, twilight
—	"2150"	—	Twilight and aurora
Solar	2000-2900	—	Numerous Fraunhofer absorption lines observed in background
—	2000-2900	O_3 Hartley continuum	Absorption in atmosphere decreases background levels
—	1300-1750	O_2 Schumann-Runge cont.	Absorption in atmosphere decreases background levels
—	1750-2050	O_2 Schumann-Runge bands	Bands observable in absorption superimposed on Rayleigh scatter level

The day maximum VUV range from 1070 to 1930 Å is displayed at a bandwidth of 5 Å with a linear intensity axis in Figure 11. Two intensity ranges are shown to illustrate better the weaker N_2 LBH bands and N lines. For interpreting which spectra to sum, the photometer records are very useful, as they can demonstrate whether spatial variation is occurring, such as in auroras. These regions can thus be identified for separate treatment, as the spectra would be expected to show possible differences between the particle excitation of an aurora and the generally less energetic photoelectron excitation.

The UV range from about 1620 to 2900 Å is shown in Figure 12 at a nominal resolution of about 1 Å. In this case, the day spectrum is dominated by the combined effects of Rayleigh scattering of sunlight and absorption of the backscattered solar radiation by atmospheric ozone. The minimum near 2500 Å is the result of

absorption in the ozone Hartley continuum, which has its maximum near this point. This absorption is the basis of a satellite remote sounding technique for ozone.[8,9]

The most striking feature of Figure 12 is the appearance of solar Fraunhofer absorption lines in the airglow. The full-disk solar spectrum[10] placed above our earth background spectrum has identical absorption lines and general shape if allowance is made for the ozone continuum. This solar spectrum was obtained with a bandwidth of 3 Å. An accurate wavelength scale has been generated from the day Fraunhofer line locations and bands observed in aurora.

At wavelengths immediately shorter than 2000 Å, several oxygen Schumann-Runge absorption bands can barely be seen. For the minimum SZA conditions such as Figure 12, no atmospheric atomic line or band emission is clearly evident in the UV spectrum, but further examination of the records may lead to an identification in the future.

Twilight observations in this near noon-midnight sun synchronous orbit are restricted to higher latitudes. Therefore, orbits must be selected that are some distance from the auroral particle excitation region to separate the two cases. These observations are being analyzed and will be reported in detail in the future. Preliminary results at 5 Å resolution clearly demonstrate that the feature in the 2140 to 2155 Å region differs in auroral and twilight spectra. These results support the recent reinterpretation of this feature in the aurora.[11,12] It has been previously considered to be the (1, 0) band of the nitric oxide gamma system at about 2150 Å.

Under nighttime conditions, the spectrometer is usually commanded to the 25 Å slits for both ranges. Hydrogen Lyman alpha is observed at all times. In the auroral regions the oxygen 1304 Å and 1356 Å multiplets, the nitrogen LBH bands, and numerous nitrogen atom emission lines appear. The 1304 Å and 1356 Å oxygen emissions again become observable in the tropical UV airglow bands. The oxygen Herzberg bands are readily observable throughout the night in the 2500 to 2900 Å region.

4. DISCUSSION

4.1 Nitrogen Lyman-Birge-Hopfield Emission

The emission of the molecular nitrogen Lyman-Birge-Hopfield (LBH) bands is a prominent feature of the day airglow in the vacuum ultraviolet. In this experiment, the bands are observed by the spectrometer during the day (Figure 11), in the auroral regions, and very weakly in the northern night sector. The LBH bands observable

---

(Because of the number of references mentioned above, they will not be listed here. *Refer to Reference Page 41, for References 8 through 12.*)

in Figure 11 are listed in Table 3; they include a few weaker bands at wavelengths longer than 1500 Å that were previously not observed.

Global levels can be obtained by the response of the 1550 Å filter as shown in Figure 8. This response is largely due to the LBH bands as shown in Table 2. The 1750 Å filter curve shown in Figure 9 is due to both LBH band emission and solar scattering. For the 1750 Å filter, the variation above the slowly changing solar scatter background is due to the LBH bands. In Figures 8 and 9, the same general enhancement of emission is seen in the auroral region as seen for the 1216 and 1340 Å filters, and there is also the variation from night to day. However, both LBH filters record a sharp decrease in background level in the southern day auroral region observed during the last part of the orbit. This observation indicates possible unsuspected complexity in the production mechanism around the auroral zone.

Both the 1550 and 1750 Å filters do not transmit the intense oxygen atom lines at 1304 Å and 1356 Å , and therefore they require no correction for this emission. Due to the large number of LBH bands, calculation of the radiance assuming no variation with wavelength is a fairly good approximation for the 1550 Å filter, although a small correction is necessary for the 1493 Å NI line and solar scatter.

The 1550 Å filter global response curve shown in Figure 8 has the smallest day maximum and night minimum radiance values of the four photometer filters. It also exhibits the largest change between the day and night levels, with a factor of over 2000 shown in the figure. The day maximum is about 1.3 kR for a SZA of 22°, and the night minimum is about 0.6 R. For comparison, typical values from the Ogo-4 ion-cell[7] sensitive between 1350 and 1550 Å are given as 2.5 kR day maximum at the subpolar point and ≤ 10 R at night outside the equatorial night airglow bands. It should be noted that the altitudes and bandpasses are different so that an exact comparison is not possible.

Our 1550 Å filter was planned to be near the predicted minimum in the day airglow background and from results shown by the photometer data, this appears to be the case. For example, the 1750 Å filter curve (Figure 9) has a day maximum of 3.7 kR and a night minimum of about 6 R. As a point of interest, it can be noted that much smaller day backgrounds are found in the spectrometer data. For example, the minimum at about 1380 Å in Figure 11 corresponds to a radiance level of ≤ 3 R/Å after correction for scattered light. The daytime maximum radiance appears to be fairly constant for different orbits. However, the night minimum tends to be variable. For the 1550 Å filter, values up to three times larger than the Figure 8 minimum have been found. For the 1750 Å filter, the minimum of 6 R in Figure 9 is one of the larger observations. The minimum is more often found to be less than 1 R.

The most striking aspect of the 1550 and 1750 Å filter curves, however, is their generally asymmetric shape. The radiance level is a minimum well before the night equator crossing and the day maximum occurs before the day equator is reached. The curve appears to be related to the SZA with the day maximum occurring at 24°, which is a few minutes before the midday minimum SZA of about 22° is reached. The night minimum occurs at about 146°, or a few minutes before maximum SZA of 158° at night. The day behavior appears to be similar to a model[13] which utilized the reciprocal of the Chapman function to fit the SZA variation in the Ogo-4 data. The present data indicate that similar behavior with respect to solar position may continue at night. This observation would appear to require an additional source beyond the ones presently considered, due to electron excitation either by solar photoelectrons in the dayglow or more energetic electrons in the auroral zones. Possibilities would include previously unobservable particle excitations or multiple-scattering from the sunlit regions. The shape of the curves may also be indicative of composition variations in the atmosphere. The satellite is decreasing in altitude from about 230 to 300 km during the enhancement, which would rule out brightening due to rising above an emitting layer.

This brightening in the night northern sector is believed to be typical. From presently available quick-look microfiche data, the brightening is observed for the 1550 Å filter in all 17 cases where the aperture is suitably large. The less extensive 1750 Å filter data exhibits the brightening in the 8 orbits with the highest sensitivity. This enhancement is typically more pronounced for the 1550 Å filter, as in Figures 8 and 9. The brightening appears due to the N_2 LBH bands from sums of 25 Å spectra for the most intense cases.

The LBH dayglow radiance measurements can be compared by obtaining the value for a nadir observation with overhead sun (SZA = 0) and from an altitude sufficient to observe the total column emission intensity. The SZA correction is based on a model developed from the Ogo-4 data.[13] For small SZA values, the model correction involves dividing the observed radiance by the cosine of the SZA. The observed radiance is also increased to include the total LBH band system. The Ogo-4 data give a value on the order of 6.5 kR[13] from an altitude of at least 400 km. A rocket measurement viewing in the upward direction to about 200 km yields a value of 3.8 kR when converted as defined.[14] A recent rocket experiment which made observations in the nadir direction from 250 km found about 2 kR.[15] The present data

13. Prinz, D.K., and Meier, R.R. (1971) Ogo-4 observations of the Lyman-Birge-Hopfield emission in the day airglow, J. Geophys. Res. 76:6146-6158.

14. Takacs, P.Z., and Feldman, P.D. (1977) Far ultraviolet atomic and molecular nitrogen emission in the dayglow, J. Geophys. Res. 82:5011-5023.

15. Strickland, D.J. (1979) Private communication.

(Figure 11) lead to an initial value of approximately 3.2 kR. The more recent measurements therefore indicate that the Ogo-4 levels should be revised to smaller backgrounds.

The altitude variation of the LBH emission is not well-defined. Some observations have indicated that one-half the emission occurs above 220 km,[14] which would require many of our observations at 260 to 160 km to be increased significantly to obtain the total column emission rate. The recent rocket measurement[15] obtained side-viewing spectra, indicating that the peak in emission rate is near 170 km. In addition, generally lower peak altitudes are found in earth limb observations[16] from the Orbiting Astronomical Observatory A-2 satellite using a 1500 Å interference filter similar to our 1550 Å filter. Analysis of these observations indicates the tangent altitude of maximum column emission to be 155, 170, and 140 km for three passes. These altitudes are expected to be near the altitude of maximum volume emission. From these results, it appears that only a small correction may be necessary for our observations. The A-2 satellite filter gives day radiance values about six times the value of 1.3 kR of our photometer (Figure 8). The difference may be due to change in sensitivity during orbit or to the sizeable correction necessary to convert the observed radiance to nadir viewing with overhead sun.

It has been demonstrated[13] from the Ogo-4 data that the emission also varies with the 10.7-cm solar flux and with season. An enhancement following solar flares has been found.[17] A more complete comparison and fit to existing models[18, 19] will require analysis of the observations for the complete flight when available.

4.2 Vacuum Ultraviolet Aurora

The presence of additional emission from aurora has been observed routinely in our data from high latitudes. These are regions of enhancement in the observed counts above the slowly-varying solar controlled airglow and scatter. The full-orbit photometer traces clearly show the effect (Figures 6, 7, 8, and 9) both for solar-illuminated and dark atmospheres.

Previous observations[7] from Ogo-4 have placed the auroral enhancement regions in the auroral oval, whose location is based on visible wavelength observations. As

16. Fishburne, E.S., Waters, C.E., Moyer, D.L., and Green, B.S. (1972) OAO, A-2 Measurements of the Ultraviolet Airglow, Final Report Contract No. F19628-71-C-0128, Report AFCRL-72-0318, AD 752228.

17. Opal, C.B. (1973) Enhancements of the photoelectron-excited dayglow during solar flares, Space Res. XIII 2:797-802.

18. Green, A.S.E., and Barth, C.A. (1967) Calculations of the photoelectron excitation of the dayglow, J. Geophys. Res. 72:3975.

19. Delgarno, A., McElroy, M.B., and Stewart, A.I. (1969) Electron impact excitation of the dayglow, J. Atmos. Sci. 26:753.

representative of the present observations, the ground tracks of the orbits of Figures 6 through 9 are plotted in Figures 13 and 14, together with the locations of enhanced VUV radiation. The north and south polar regions are given on separate plots. The ground tracks have been converted to corrected geomagnetic latitude and corrected local geomagnetic time.[20] The auroral oval for the magnetic index Q = 3 has been included.[21]

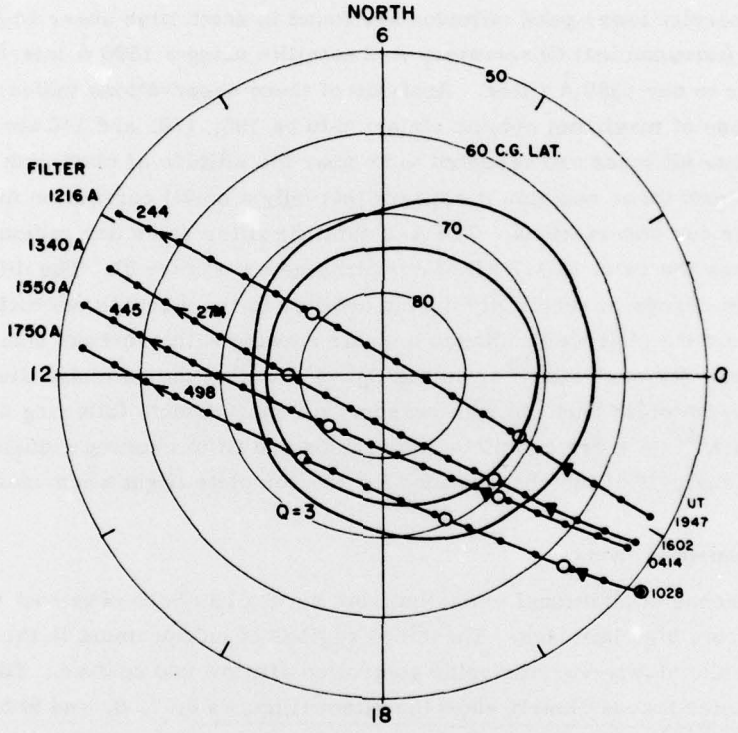

Figure 13. Auroral Oval and Global Survey Tracks: North Polar Region

The oval location can help make understandable numerous features of the photometer traces, as a comparison of Figures 6 through 9 and Figures 13 and 14 will reveal. As the earth turns under the sun-synchronous satellite, a wide range

20. Gustafsson, G. (1969) A revised corrected geomagnetic coordinate system, Arkiv Geofysik 5:595-617.

21. Feldstein, Y.I., and Starkov, G.V. (1967) Dynamics of auroral belt and polar geomagnetic disturbances, Planet. Space Sci. 15:209-229.

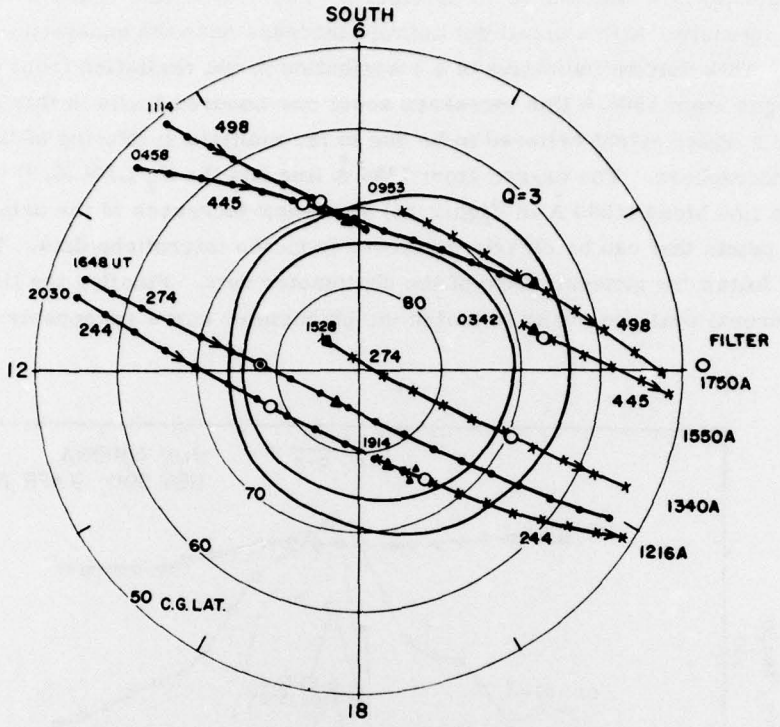

Figure 14. Auroral Oval and Global Survey Tracks: South Polar Region

of oval crossings is possible. On some passes, the track is somewhat along the oval (Rev 498), giving an extended enhanced region. A track across a smaller portion of the oval gives a sharper enhancement. The oval is based on observation frequencies so that it describes many but not all observations. The limits are not well-defined, but are partly due to sensitivity limits. The match shown in Figures 13 and 14, together with about thirty other similar cases we have observed, leaves no doubt that aurora are being observed and also that the VUV can be used to readily detect and study aurora both night and day.

The use of both the photometer and spectrometer for auroral investigations is shown in Figure 15. One of the strongest night aurora observed to date is seen by the 1550 Å filter of the photometer. The increase above the local background is about three orders of magnitude. The average curve is drawn through the individual points, not shown in the figure. During this period, the spectrometer sampled each wavelength in the 1100 to 2900 Å region at least every 22 seconds. Some of these

measurements are also shown on the figure. The 1216 Å line remains almost constant in intensity, with a small but definite increase near the equatorial side of the aurora. This may be indicative of a contribution to the excitation from protons. The oxygen atom 1304 Å line increases about one-hundred times in this region. It also has a wider extent believed to be due to the multiple scattering of this radiation in the atmosphere. The oxygen atom 1356 Å line and the N_2 LBH (3, 3) band-atomic nitrogen line blend (1500 Å in Figure 15) also show increases at the same time for the few points that can be clearly measured from the microfiche data. These lines roughly follow the general shape of the photometer data. Finally, the limits of the Q = 3 auroral oval are shown to match the photometer curve reasonably well.

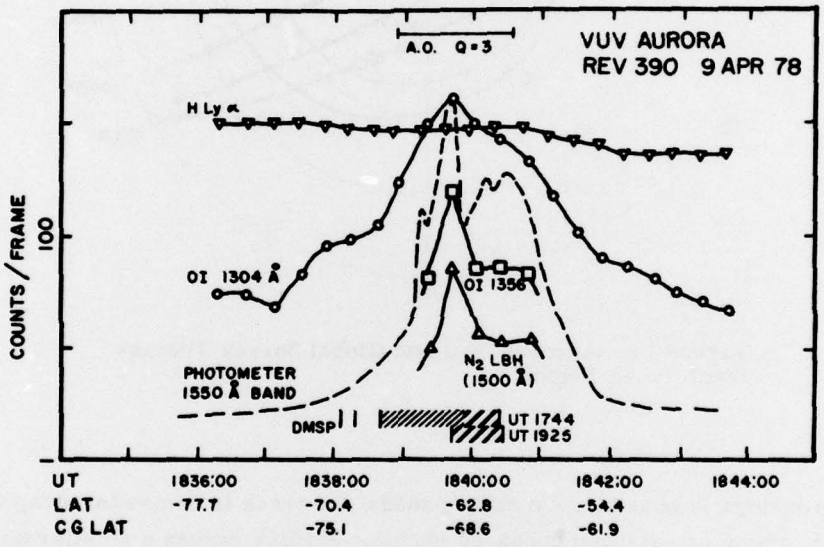

Figure 15. Vacuum Ultraviolet Aurora: Spectrometer, Photometer, and DMSP Satellite Combined Observations

The spatial resolution in Figure 15 for the photometer corresponds to a FOV diameter of 5.9° or about 10 km for radiation from an altitude of 100 km with the satellite at 200 km. One FOV is traversed in about 1.4 sec so that there are about 16 photometer spatial resolution lengths between each spectrometer point. For the same altitudes, the f/5 spectrometer observes a region about 20 km square and it requires about 2.7 sec to move across this distance.

The narrow intense structure on the polar side might be characterized as a group of arcs, whereas the less structured region on the equator side appears to be

similar to diffuse aurora. It is possible to fit one or several Gaussian curves reasonably well to the profile in this region.[4]

The observations on this experiment also correlate reasonably well with auroral locations found from spatial images taken by a Defense Meteorological Support Program satellite. Visible region aurora may be clearly seen in many of these images.[22] The locations of auroral arcs (vertical lines) and more diffuse regions (hatch marks) are shown for passes in the same general region about one hour before and 45 min after the present observations.[23] It is not expected that forms changing rapidly during the approximately one-hour intervals will be correlatable between these observations, but the detection of the less rapidly changing diffuse regions at the same general location tends to support the reasonably close association of VUV and visible aurora.

These results demonstrate the use of VUV sensors for detection and study of the aurora. One unique feature of the VUV is the fact that solar-illuminated, or daytime, aurora can be investigated. Further analysis of the present results should allow better definition of the most suitable bands for day and night auroral detection using topside remote sensing or imaging.

4.3 Hydrogen Lyman-alpha Geocorona

The variation of hydrogen Lyman-alpha radiance over the total orbit is shown in Figure 6 for the 1216 Å filter. Note that the variation from night to day is not as extreme as in some of the other bands. This filter observed primarily the hydrogen Lyman alpha line at 1216 Å, but the oxygen atom triplet centered at 1304 Å is observed with about half the filter sensitivity (Figure 5). Except for the night mid-latitude region, both lines are always present. Indeed, during the day maximum at the smallest solar zenith angle, the 1304 Å line is usually stronger than 1216 Å. Well developed aurora are present in the day and night south polar region and in the north daytime region. A relatively small tropical airglow due to atomic oxygen emission is observable. In both of these cases, spectrometer observations show that the increase is due solely to oxygen.

From spectra taken with the 25 Å bandwidth at the same time as the records in Figure 6, the day maximum airglow has been separated into contributions from both lines. The 1356 Å line makes only a minor contribution with this filter and therefore has been neglected. The maximum H Lyman alpha radiance is 13 kR and the 1304 Å value is 18 kR. With use of the spectrometer lines themselves, these levels are found to be 14 and 18 kR, respectively. These values refer to the minimum SZA

22. Pike, C. P., and Whalen, J. A. (1974) Satellite observations of auroral substorms, J. Geophys. Res. 79:985-1000.

23. Whalen, J. A. (1978) Private communication.

of about 22°. There is not a strong variation with SZA near the minimum value. The observed night minimum 1216 Å intensity outside the tropical airglow belt is about 0.5 kR.

The 1216 Å geocoronal hydrogen airglow near the earth has been measured many times[24, 25, 26] from relatively low altitudes and modeled under the assumption of multiple solar resonance scattering.[25, 26, 27] This multiple scattering leads to a fairly high radiance level at night, as well as during the day, since solar radiation is scattered into the dark side of the earth. The intensity maximum is approximately centered near the smallest solar zenith angle. The resonance scattering extends to several earth radii[28] and the present observation at altitudes near 200 km includes only the radiation emitted in the lower portion of the scattering region. Therefore, these measurements should be useful in improving the model for applications well within the geocorona.

Combined Ogo-4 and Oso-4 results give a day nadir-viewing maximum of about 20 to 25 kR and a night value of about 1 kR.[25] The levels reported here are considerably lower. However, the measured intensity depends on the altitude and solar flux level, as well as the SZA. For example, the model in Reference 25 (Figures 13 and 14) shows about a 15 percent decrease in nadir radiance from Ogo-4 and Oso-4 altitudes near 650 km to 215 km. Our day altitude near 180 km should reduce it further, although it appears that our levels are still less than the earlier work. A rocket observation[29] with altitude comparable to the present observation gives about 13 kR for 1216 Å, 7 kR for 1304 Å, and 0.4 kR for 1356 Å.

4.4 Oxygen Tropical UV Airglow

The equatorial enhancement of the oxygen multiplets commonly referred to as the 1304 and 1356 Å lines (see Table 3) was first observed by the Ogo-4 satellite[30, 31] and clear images of it were obtained during the Apollo 16 mission.[32] This airglow is readily seen by the present experiment. The 1340 Å filter curve in Figure 7 shows prominent tropical structure and a small enhancement is seen in the 1216 Å filter curve in Figure 6 as well. These regions of increased emission are due to increases in the oxygen atom emission only as found by spectrometer data such as that shown in Figure 16. Near the equatorial region, the oxygen 1304 Å and in some cases the oxygen 1356 Å lines can be clearly seen to increase in intensity.

Observations from Ogo-4 indicated usually two maxima approximately the same distance north and south of the magnetic dip equator with the largest maximum to the south. Ogo-4 also found variation in the intensity of the airglow on each pass. We find the same general behavior, as seen in Figures 7 and 17, although there

---

(Because of the number of references mentioned above, they will not be listed here. Refer to Reference Page 41, for References 24 through 32.)

appears to be structure within the bands. One of the strongest airglows to date is shown in Figure 17, which is a photometer record. When the photometer 1340 Å filter is not in use, the airglow can still usually be observed at the 1304 Å line with the spectrometer. The repetitive scan results in an observation every 22 sec or about 1.5° of latitude.

Our measurements cover the time period from the end of March to mid-September, 1978, or approximately from the vernal to the autumnal equinox at the near constant local time of about 2230 hours. Therefore the present observations when completely reduced should allow an assessment of the seasonal effect for a fixed local time. This effect if present is difficult to separate from local time effects in the Ogo-4 data, since local time of observation varied throughout the flight. Our fixed local time is fortunately near the time of the maximum airglow.[30,31]

Our nadir-viewing observations from 220 ± 20 km are different both in intensity and in relative wavelength distribution from previous observations.[31] Previously, the ratio of the 1304 Å to the 1356 Å line intensities for a large number of observations was about 1.8. We find the 1356 Å line to be much weaker and in many cases it is almost unobservable on a single spectrometer scan. Figure 16 is typical in this regard. The 1304/1356 ratio is generally between 10 and 20. Previous measurements[31] found a range of about 300-1500 R for 1304 and about 200-800 R for 1356. For two of our stronger cases in Figure 7 and Figure 17 we find 120 R (Southerly) and 30 R (Northerly) and 170 R (S) and 20 R (N), respectively, for what is almost exclusively 1304 Å radiation.

It is probable that the large difference in these observations is mainly due to the difference in our altitude of about 220 km and the Ogo-4 altitude of from about 450 to 650 km. The previous observations included the complete night F-layer, whereas the present observations are below the usual altitude range of the night F-layer. The source of the tropical UV airglow in the F-region is generally considered to be radiative recombination; although ion-ion recombination and soft electron collisional excitation have also been considered. Oxygen ion radiative recombination is usually not considered competitive with ion-molecule or charge exchange reactions at the lower altitudes of the present observations. However, radiative deexcitation is competitive with collisional deexcitation throughout this region, since the spin-forbidden 1356 Å transition (Table 3) has the fairly short radiative lifetime[33] of 6×10^{-4} sec. Most other commonly invoked reactions such as dissociative recombination of O_2^+ or NO^+ are not exothermic enough to yield the upper states of the 1304 or 1356 Å radiation.

---

33. Lawrence, G. M. (1969) Vacuum ultraviolet transition probabilities in C, N, O, and N_2, Can. J. Chem. 47:1856-1857; Phys. Rev. 2A:397-407 (1970) Dissociative excitation of some oxygen-containing molecules: Lifetimes and electron-impact cross-sections.

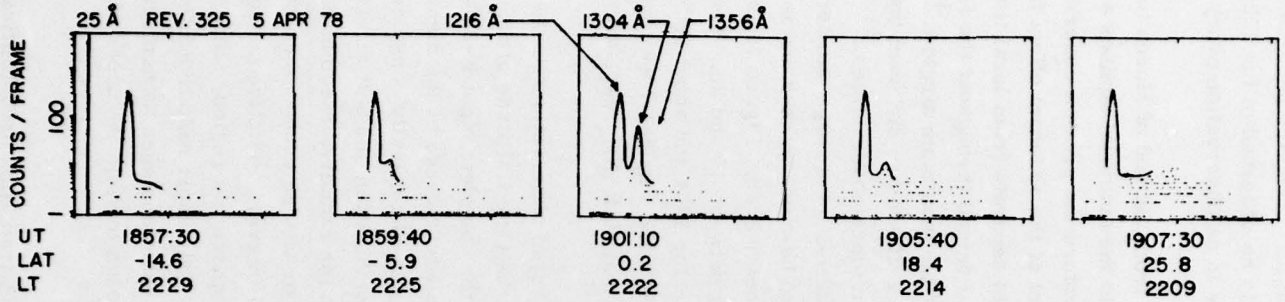

Figure 16. Tropical UV Airglow Observed by Spectrometer

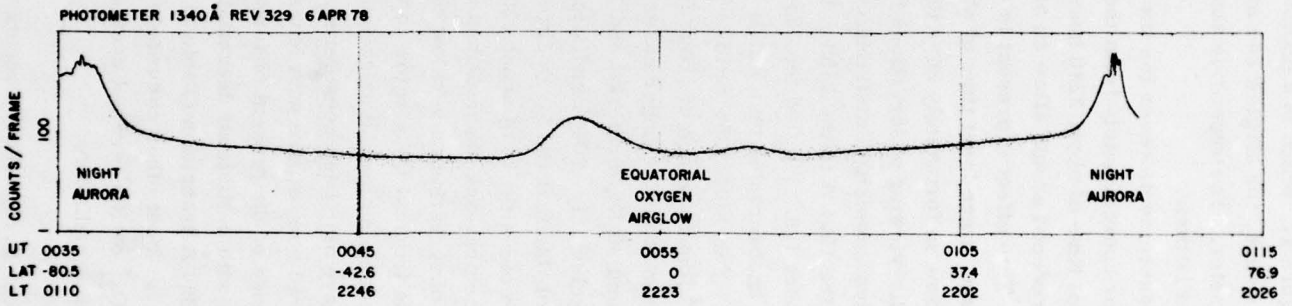

Figure 17. Tropical UV Airglow Observed by Photometer (1340 Å Filter)

A possible explanation for the emission is that it originates in the F layer, probably by radiative recombination, and then undergoes multiple scattering so that a certain fraction of the radiation is visible below our altitude. In this regard, the 1356 Å radiation would be more affected by absorption due to molecular oxygen because of its weaker self-absorption, resulting in a longer mean path for possible removal by oxygen molecule absorption.

One point that can be made from the present observations is that the use of the 1356 Å oxygen line in techniques[34,35,36] to sense remotely the F-region is made more attractive by our observation of very weak 1356 Å apparent column emission rates below 220 km. This observation indicates that there will not be appreciable interference from 1356 Å radiation at lower altitudes.

Similar emission has been reported in the day equatorial region,[30] but it has not been clearly identified in our data at present. Radiative recombination emission has been seen at mid-latitude by rocket,[37] but it originates above 220 km and thus could not be seen by our instruments.

A number of observations were made at night using the 1340 Å filter on the three consecutive passes closest to Kwajalein during the DNA Wideband Support program planned launches. The primary sensor on the S3-4 platform for these tests was the NRL pulsed plasma probe. The goal was to obtain data from the Wideband satellite experiment, the Altair incoherent scatter radar, instrumented sounding rockets, and S3-4. Although the rockets did not achieve desired altitudes, our planned data records were obtained. The tropical airglow radiation was not certain to be observable due to the relatively low altitude; however, results given herein demonstrate measurable oxygen line enhancements. Therefore, these data, when available, will be correlated with the other observations to see if any evidence of irregularity development and striations leading to scintillations and other effects on satellite communications can be observed.

---

34. Meier, R. R., and Opal, C. B. (1973) Tropical UV arcs: Comparison of brightness with f_0F_2, J. Geophys. Res. 78:3189-3193.

35. Chandra, S., Reed, E. I., Meier, R. R., Opal, C. B., and Hicks, G. T. (1975) Remote sensing of the ionospheric F layer by use of OI 6300 Å and OI 1356 Å observations, J. Geophys. Res. 80:2327-2332.

36. Tinsley, B. A., and Bittencourt, J. A. (1975) Determination of F region height and peak electron density at night using airglow emissions from atomic oxygen, J. Geophys. Res. 80:2333-2337.

37. Brune, W. H., Feldman, P. D., Anderson, R. C., Fastie, W. G., and Henry, R. C., (1978) Midlatitude oxygen ultraviolet airglow, Geophys. Res. Lett. 5:383-386.

5. CONCLUSIONS

The initial observations from the available data, described in detail in this report, amply demonstrate the importance of atmospheric ultraviolet radiation observations to the goals of numerous DOD applications. Lower levels of day and night backgrounds found here must be included in future assessments of missile surveillance and tracking systems. Although not optimized for remote sensing or auroral detection, the data are applicable in studies related to atmospheric species densities, continuous aurora, over-the-horizon radar, and atmospheric nuclear effects. There are many potential uses for ultraviolet remote sensing, including horizon determination, spatial images of disturbed regions and technical intelligence systems. These systems cannot be blinded from the ground due to the impossibility of penetrating the lower atmosphere with vacuum ultraviolet radiation.

References

1. Draper, J.S., Bien, F., Huffman, R.E., and Paulsen, D.E. (1975) Rocket plumes in the thermosphere, AIAA Journal 13:825-827.
2. Russak, S.L., Flemming, J.C., Huffman, R.E., Paulsen, D.E., and Larrabee, J.C. (1979) Development of Proximity and Electrostatically Focused Digicons for UV Measurements from Sounding Rockets, AFGL-TR-79-0006, AD A068086.
3. Marcos, F.A., and Champion, K.S.W. (1979) Satellite Density Measurements with the Rotatable Calibration Accelerometer (ROCA), AFGL-TR-79-005, AD A069740.
4. Whalen, J.A., and Sharber, J.R. (1979) Integration over the loss cone of electrons in the continuous (diffuse) aurora: Gaussian latitudinal profile, Trans. Am. Geophys. Union 60:355.
5. Szuszczewicz, E.P., Holmes, J.C., and Walker, D.N. (1979) On the probing of ion and electron irregularity spectra, Trans. Am. Geophys. Union 60:339.
6. Barth, C.A., and Mackey, E.F. (1969) Ogo-4 ultraviolet airglow spectrometer, IEEE Trans. on Geoscience Electronics GE7(2):114-119
7. Chubb, T.A., and Hicks, G.T. (1970) Observations of the aurora in the far ultraviolet from OGO-4, J. Geophys. Res. 75:1290-1311.
8. Rawcliffe, R.D., and Elliott, D.D. (1966) Latitude distributions of ozone at high altitudes deduced from satellite measurement of the earth's radiance at 2840 Å, J. Geophys. Res. 71:5077-5089.
9. Heath, D.F., Mateer, C.L., and Krueger, A.J. (1973) The Nimbus-5 back-scatter ultraviolet (BUV) atmospheric ozone experiment — two years operation, Pure and Appl. Geophys. 106-108:1238-1253.
10. Broadfoot, A.L. (1972) The solar spectrum 2100-3200 Å, Astrophys. J. 173:681-689.
11. Beiting, E.J., and Feldman, P.D. (1978) A search for nitric oxide gamma band emission in an aurora, Geophys. Res. Lett. 5:51.

References

12. Dick, K. A. (1978) The auroral 2150 feature: A contribution from lines of single ionized atomic nitrogen, Geophys. Res. Lett. 5:273.

13. Prinz, D.K., and Meier, R.R. (1971) Ogo-4 observations of the Lyman-Birge-Hopfield emission in the day airglow, J. Geophys. Res. 76:6146-6158.

14. Takacs, P.Z., and Feldman, P.D. (1977) Far ultraviolet atomic and molecular nitrogen emission in the dayglow, J. Geophys. Res. 82:5011-5023.

15. Strickland, D.J. (1979) Private communication.

16. Fishburne, E.S., Waters, C.E., Moyer, D.L., and Green, B.S. (1972) OAO, A-2 Measurements of the Ultraviolet Airglow, Final Report Contract No. F19628-71-C-0129, Report AFCRL-72-0318, AD 752228.

17. Opal, C.B. (1973) Enhancements of the photoelectron-excited dayglow during solar flares, Space Res. XIII 2:797-802.

18. Green, A.E.S., and Barth, C.A. (1967) Calculations of the photoelectron excitation of the dayglow, J. Geophys. Res. 72:3975.

19. Dalgarno, A., McElroy, M.B., and Stewart, A.I. (1969) Electron impact excitation of the dayglow, J. Atmos. Sci. 26:753.

20. Gustafsson, G. (1969) A revised corrected geomagnetic coordinate system, Arkiv Geofysik 5:595-617.

21. Feldstein, Y.I., and Starkov, G.V. (1967) Dynamics of auroral belt and polar geomagnetic disturbances, Planet. Space Sci. 15:209-229.

22. Pike, C.P., and Whalen, J.A. (1974) Satellite observations of auroral substorms, J. Geophys. Res. 79:985-1000.

23. Whalen, J.A. (1978) Private communication.

24. Wallace, L., Barth, C.A., Pearce, J.B., Kelly, K.K., Anderson, D.E., Jr., and Fastie, W.G. (1970) Mariner 5 measurements of the Earth's Lyman alpha emission, J. Geophys. Res. 75:3769-3777.

25. Meier, R.R., and Mange, P. (1970) Geocoronal hydrogen: An analysis of the Lyman alpha airglow observed from Ogo-4, Planet. Space Sci. 18:803.

26. Thomas, G.E. (1963) Lyman alpha scattering in the Earth's hydrogen geocorona, J. Geophys. Res. 68:2639.

27. Meier, R.R., and Mange, P. (1973) Spatial and temporal variations of the Lyman alpha airglow and related atomic hydrogen distributions, Planet. Space Sci. 21:309-327.

28. Carruthers, G.R., Page, T., and Meier, R.R. (1976) Apollo 16 Lyman-alpha imagery of the hydrogen geocorona, J. Geophys. Res. 81:1664-1672.

29. Fastie, W.G., Crosswhite, H., and Heath, D. (1964) Rocket spectrometer airglow measurements in the far ultraviolet, J. Geophys. Res. 69:4129-4140.

30. Hicks, G.T., and Chubb, T.A. (1970) Equatorial auroral airglow in the far ultraviolet, J. Geophys. Res. 75:6233-6248.

31. Barth, C.A., and Schaffner, S. (1970) Ogo-4 spectrometer measurements of the tropical ultraviolet airglow, J. Geophys. Res. 75:4299-4306.

32. Carruthers, G.R., and Page, T. (1976) Apollo 16 far ultraviolet imagery for the polar auroras, tropical airglow belts, and general airglow, J. Geophys. Res. 81:483-496.

33. Lawrence, G. M. (1969) Vacuum ultraviolet transition probabilities in C, N, O, and N_2, Can. J. Chem. 47:1856-1857; Phys. Rev. 2A:397-407 (1970) Dissociative excitation of some oxygen-containing molecules: Lifetimes and electron-impact cross-sections.

34. Meier, R. R., and Opal, C. B. (1973) Tropical UV arcs: Comparison of brightness with f_0F_2, J. Geophys. Res. 78:3189-3193.

35. Chandra, S., Reed, E. I., Meier, R. R., Opal, C. B., and Hicks, G. T. (1975) Remote sensing of the ionospheric F layer by use of OI 6300 Å and OI 1356 Å observations, J. Geophys. Res. 80:2327-2332.

36. Tinsley, B. A., and Bittencourt, J. A. (1975) Determination of F region height and peak electron density at night using airglow emissions from atomic oxygen, J. Geophys. Res. 80:2333-2337.

37. Brune, W. H., Feldman, P. D., Anderson, R. C., Fastie, W. G., and Henry, R. C. (1978) Midlatitude oxygen ultraviolet airglow, Geophys. Res. Lett. 5:383-386.